energies

MDPI

Supplementary material

Simplified 1D incompressible two-fluid model with artificial diffusion for slug flow capturing in horizontal and nearly horizontal pipes

Arianna Bonzanini [1], Davide Picchi [2] and Pietro Poesio[1,*]

[1] Dipartimento di Ingegneria Meccanica ed Industriale, Università degli Studi di Brescia, Via Branze, 38, 25123 Brescia, Italy; a.bonzanini001@unibs.it

[2] Stanford University, Energy Resources Engineering, Stanford, CA 94305, USA; dpicchi@stanford.edu

* Correspondence: pietro.poesio@unibs.it; Tel.: +39-030-371-5646

1. Further information on the numerical method

1.1. Mass conservation

The implemented numerical procedure has a little effect on the mass conservation since the threshold is very close to unity. In our model, the fluids are assumed to be incompressible, and, therefore, when a liquid slug exits the pipe a rapid change in the mass fluxes at the pipe outlet takes place. As a consequence, the integration error of the mass fluxes gives unphysical results. However, in every local section of the pipe the sum of superficial velocities (in the stratified region i.e. bubble) and the velocity of the liquid slug should be equal to the mixture velocity (to ensure the volume conservation). In Figure 1 (top) the ratio between the liquid velocity u_l and the mixture velocity U_m is plotted for a representative simulation showing that the ratio u_l/U_m is unitary in the liquid slug, i.e. $u_l = U_m$: thus, the threshold does not affect the imposed flow rates. Note that this condition is always satisfied in the stratified region.

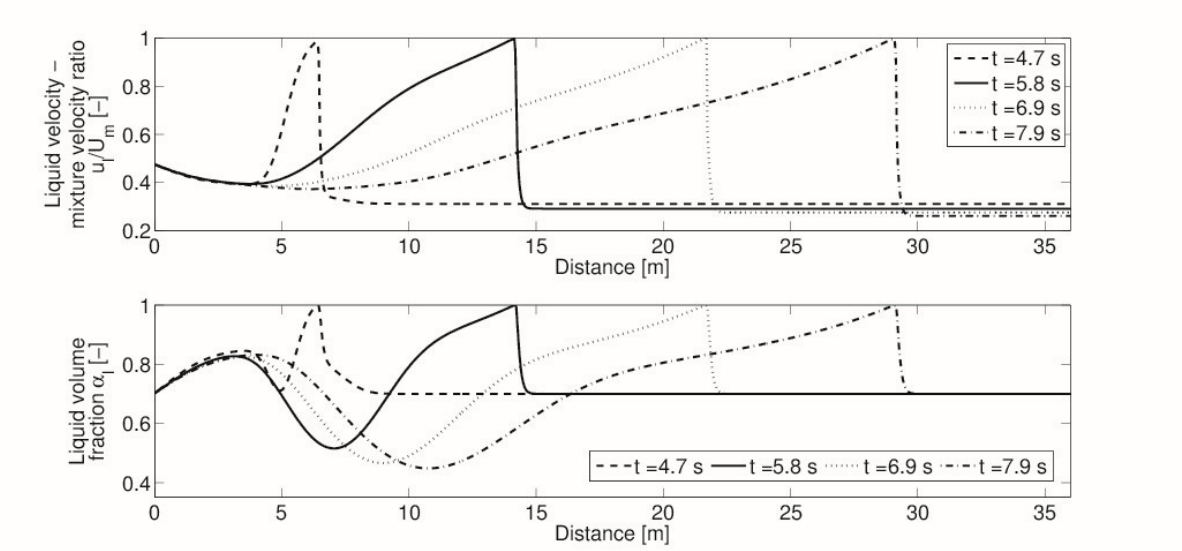

Figure 1. Time evolution of liquid velocity and mixture velocity ratio (top) and liquid volume fraction (bottom) in a slug body; $u_{ls} = 1.0\ m/s$, $u_{gs} = 2.0\ m/s$. The liquid velocity equals the mixture velocity ($U_m = 3.0\ m/s$) when the liquid volume fraction is close to unity.

1.2. Validation of the transition criterion: water air separation test

The water air separation test has been proposed in [1] and has been employed as a benchmarking test for the numerical description of phase appearance/disappearance [2-4]. The geometry consists in a 7.5 m long pipe, closed at both ends, initially filled with a uniform mixture of

air and water ($\alpha_l = 0.5,\ \rho_l = 1000\ kg/m^3,\ \mu_l = 10^{-3}\ Pa \cdot s,\ \rho_g = 1\ kg/m^3,\ \mu_g = 1.8 \cdot 10^{-5}\ Pa \cdot s$ and the system is considered as isothermal). At the beginning of the simulation, phase velocities are null; then, the two phases separates under the effect of gravity. This test shows the capability of the transition criterion in presence of phase appearance/disappearance phenomena, which takes place thanks to the phase separation process.

Figure 2 shows the time evolution of the liquid volume fraction: the test has been performed using a number of cells N = 2500, and a CFL = 0.95. It is possible to observe that two fronts appear and they merge at the pipe centre, creating a sharp interface. Figure 3 shows a grid refinement analysis of the liquid volume fraction at $t = 2\ s$: as the number of cells increases, the phase interface becomes sharper and converges toward the reference solution.

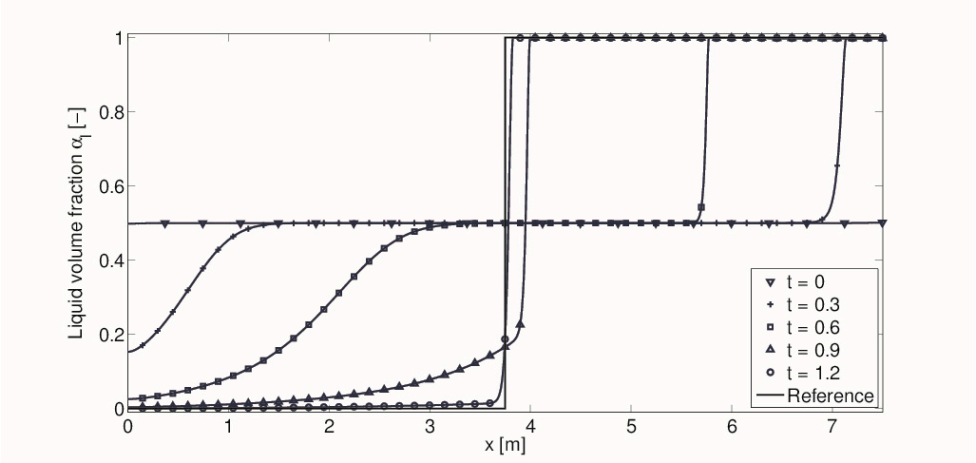

Figure 2. Phase separation test: liquid volume fraction time evolution.

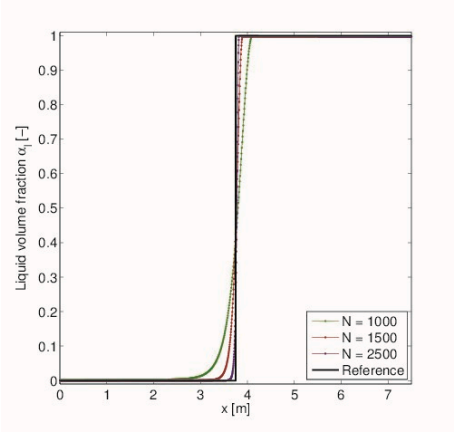

Figure 3. Phase separation test: grid refinement analysis at time $t = 2\ s$.

1.3. A possible high-order extension

The FLIC (Flux Limited Centred) scheme has been also implemented: this high-order TVD extension of the FORCE scheme can be found in [5]. The lax-Wendroff flux is employed as high-order flux, while the mean of the Lax-Friedrichs and of the Lax-Wendroff scheme is used as low-order; the adopted limiter is the Minbee. Numerical simulations on *Pipe2* are performed to observe slug characteristics and computational performances. It has been observed that the computational cost increases significantly, if compared to the one of the code without this TVD extension. Figure 4 (a) shows the dimensionless computational time of simulation performed with the TVD extension, while Figure 4 (b) shows it for simulations performed with the FORCE scheme, keeping all the other parameters (initial and inlet conditions, spatial discretisation, CFL, end time) fixed: it can be observed that the dimensionless computational time increases sensibly. This is due to

changes in the eigenvalues, given by modifications in the liquid volume fraction and velocity: as the maximum eigenvalue increases, the corresponding time step reduces, keeping the CFL constant.

The presented code modified with the high-order fluxes does not provide better results, wheter compared to the numerical solution obtained by the FORCE scheme. Figure 5 compares the computed slug mean frequency (a) and mean velocity (b) against empirical correlation, in the case of geometry *Pipe2*, for different couples of gas and liquid superficial velocities. These results are similar to the ones obtained by the FORCE scheme and presented in the paper, since the slug mean velocity is within the ± 20% bounds while, in the case of slug mean frequency, several points are outside the ± 30% bounds.

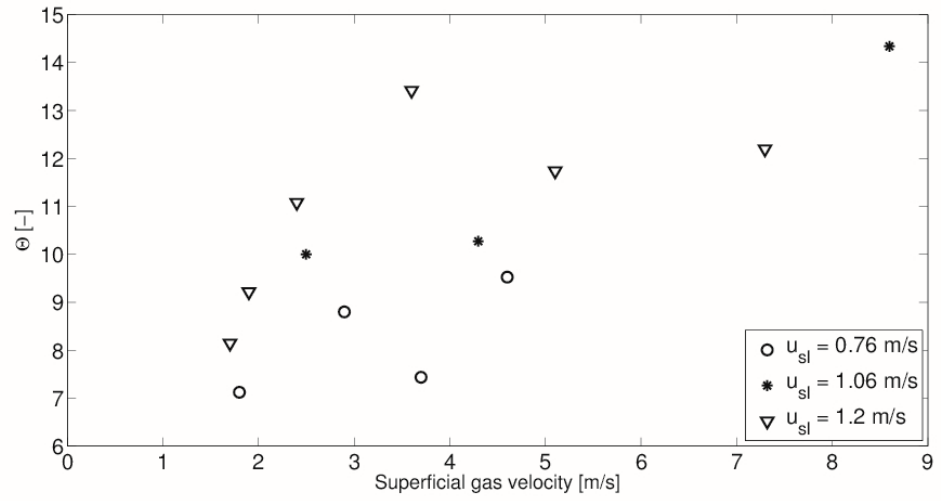

(**a**)

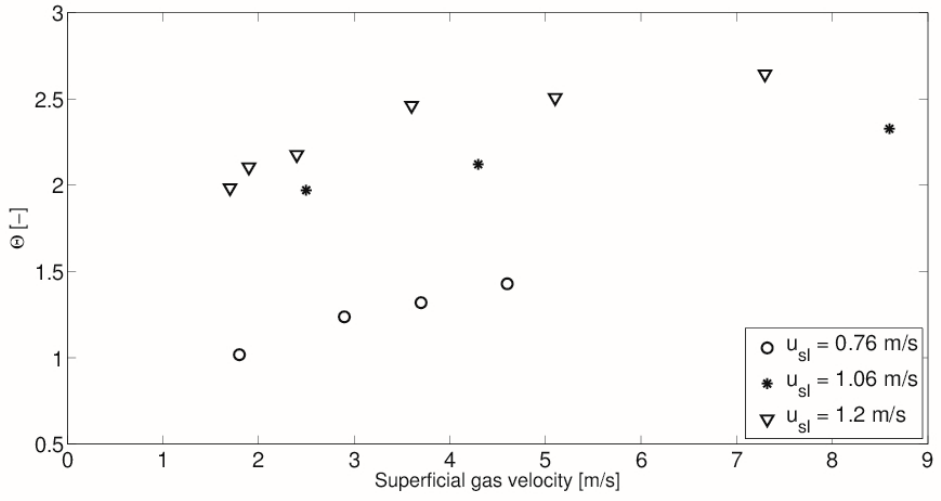

(**b**)

Figure 4. Dimensionless computational time Θ as function of the superficial gas velocity for the simulations performed on *Pipe2* with the FLIC scheme (**a**) and with the FORCE scheme (**b**) [5]: simulations with the lower superficial velocities are performed faster than real time in the case of the FORCE scheme, while the computational time increases from two to seven times more in the case of the FLIC scheme. End time $t = 300$, $\Delta x = D/2$, CFL = 0.95.

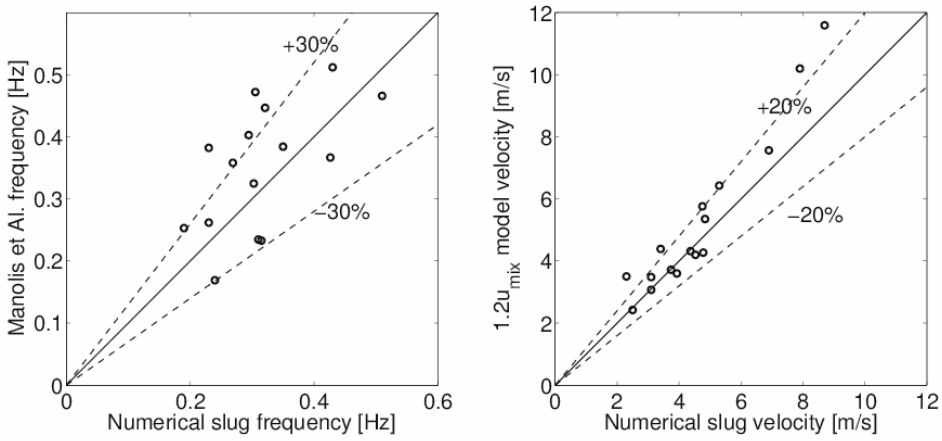

(**a**) (**b**)

Figure 5. Slug mean characteristics: frequency (**a**) and velocity (**b**) are compared against empirical models.

2. Validation against an experimental flow pattern map

In Figure 6 (a), numerical results are validated with experimental data reported in [6]. The geometry consists in a horizontal *3 m* long pipe, with an internal diameter of *0.0255 m*. The transition from smooth stratified to wavy stratified flow is well predicted; in the upper left-hand side of the map, the elongated bubble flow was experimentally recognized and distinct from slug flow (the difference between the two flow regimes consists in the gas entrainment in the liquid slug, which is absent in the first one and present in the second one); the presented numerical method cannot discern between elongated bubble and slug flow, since gas entrainment is not taken into account: thus, it was not possible to observe numerically the elongated bubble flow, instead we observed a gradual transition from smooth stratified to wavy stratified, and finally to slug flow. Barnea et al. [6] observed experimentally a sharp transition from smooth stratified to slug flow, as can be observed in Figure 6 (b). Instead, on our flow pattern map, some numerical simulations reported the wavy stratified flow above the transition line between smooth stratified and slug flow, indicating a smoother transition between these two flow regimes.

Even if some discrepancies are present between experimental data and numerical results (see Figure 6), these are acceptable for engineering applications.

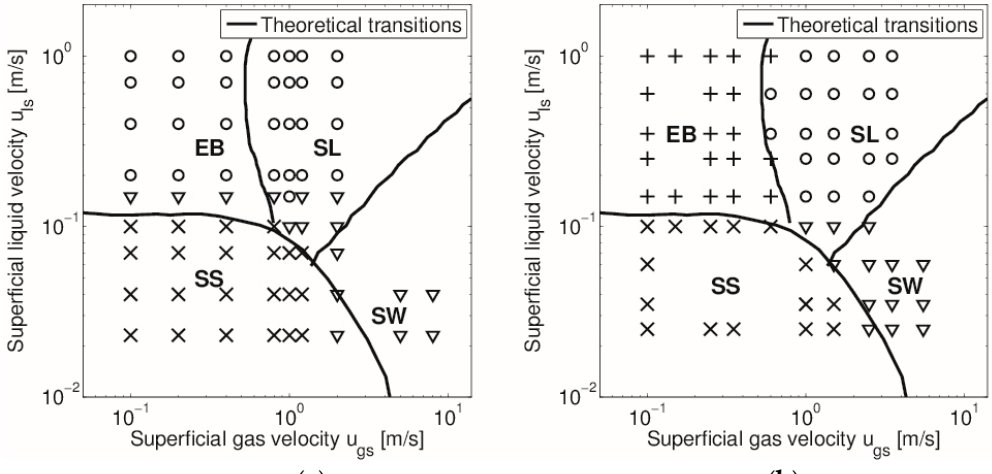

(**a**) (**b**)

Figure 6. Flow pattern map: comparison of numerical results (**a**) and experimental points (**b**). ×: Smooth stratified flow (SS), ∇: Wavy stratified flow (SW), +: Elongated bubble flow (EB), ○: Slug flow (SL).

3. Effect of grid refinement and threshold variation on slug characteristics

In this Section we investigate how the grid discretisation and the threshold value, adopted in the transition from two-phase to single phase flow criterion, affect slug mean frequency and slug mean velocity.

Figure 7 reports the threshold effects on slug statistic for three different couples of superficial velocities (simulations were performed on *Pipe2*): it is clear that the threshold value little affects slug characteristics. In our numerical simulation we set the threshold value equal to 0.999.

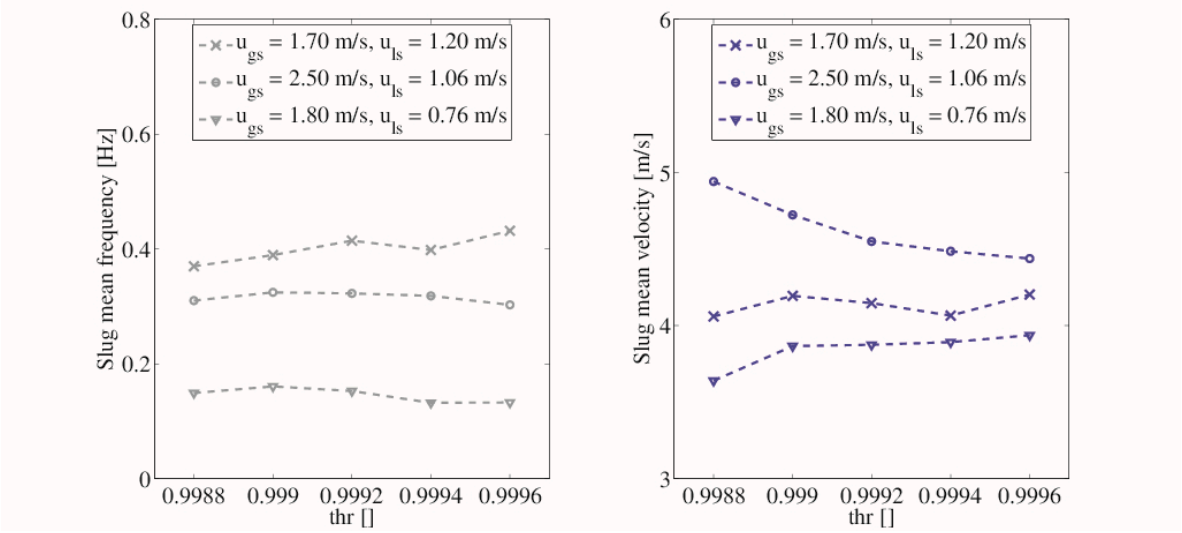

(**a**) (**b**)

Figure 7. Slug mean frequency (**a**) and slug mean velocity (**b**) as function of the threshold value for different couples of superficial velocities.

In Figure 8, slug mean frequency and velocity are reported as function of the grid discretisation. Since the coefficients of the artificial diffusion matrix were set in such a way that all the wavelengths shorter than a pipe diameter are damped, we can observe that as the grid is refined with $\Delta x \leq D/2$ slug characteristics are little affected, because all the instabilities smaller than the representative diameter are damped.

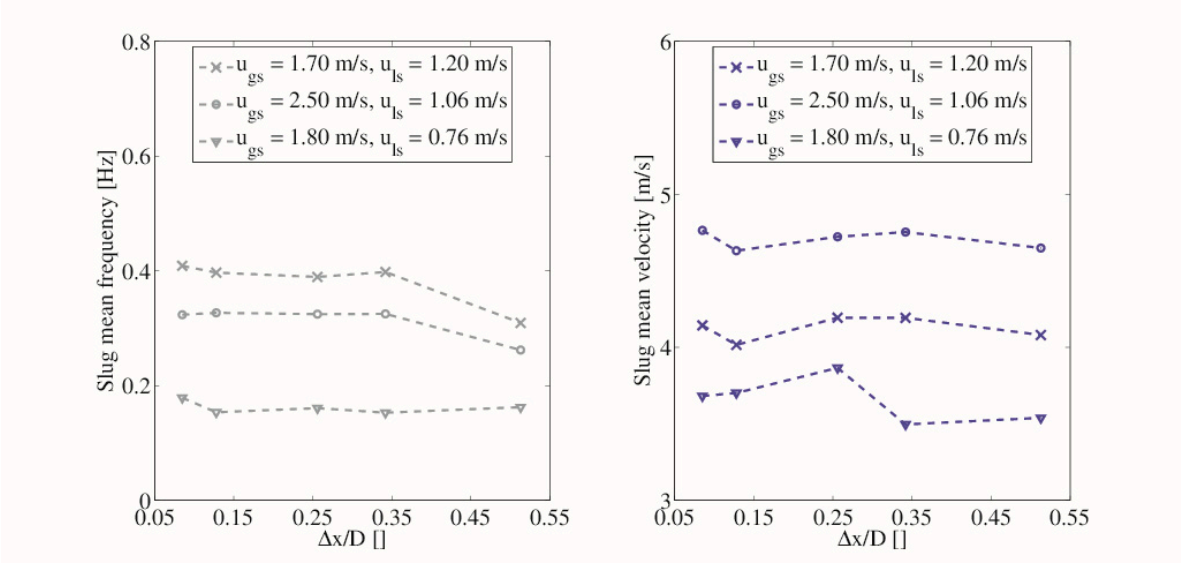

(**a**) (**b**)

Figure 8. Slug mean frequency (**a**) and slug mean velocity (**b**) as function of grid discretisation for different couples of superficial velocities.

In Table 1 are reported, for each of the analyzed couple of superficial velocities, the percentage error between the finest and the coarsest grid and between the smallest and the greatest threshold.

Table 1. Effect of grid refinement and threshold on slug mean frequency and velocity: error between the finest and the coarsest grid and between the smallest and the greatest threshold.

u_{gs}, u_{ls} $[m/s]$	Characteristic	Threshold error [%]	Grid error [%]
1.70, 1.20	Frequency	14.3	24.3
	Velocity	3.4	1.5
2.50, 1.06	Frequency	2.6	19.0
	Velocity	10.1	2.4
1.80, 0.76	Frequency	11.1	9.1
	Velocity	7.5	3.9

4. Slug initiation

Ansari [7] and Ansari and Shokri [8] recognized three main zones in slug flow initiation: a first zone, where the interface of the two-phase flow is pushed down slightly because of gas flow; a second zone, where a few waves form with short wavelengths; then, in the third zone, one of these short waves grows and finally becomes a slug. Figure 9 (a) shows slug initiation in *Pipe1* while Figure 9 (b) regards *Pipe2*. Slug initiation phenomenology is well-simulated by the proposed code, since the aforementioned three regions can be clearly identified.

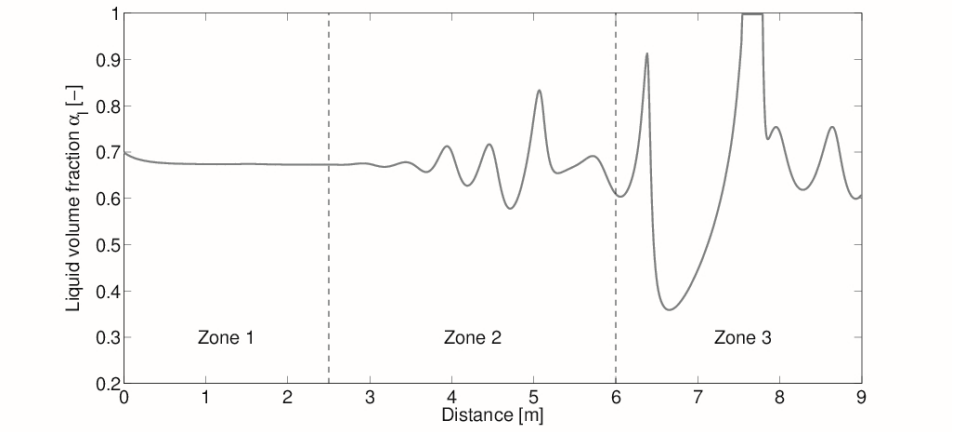

(a)

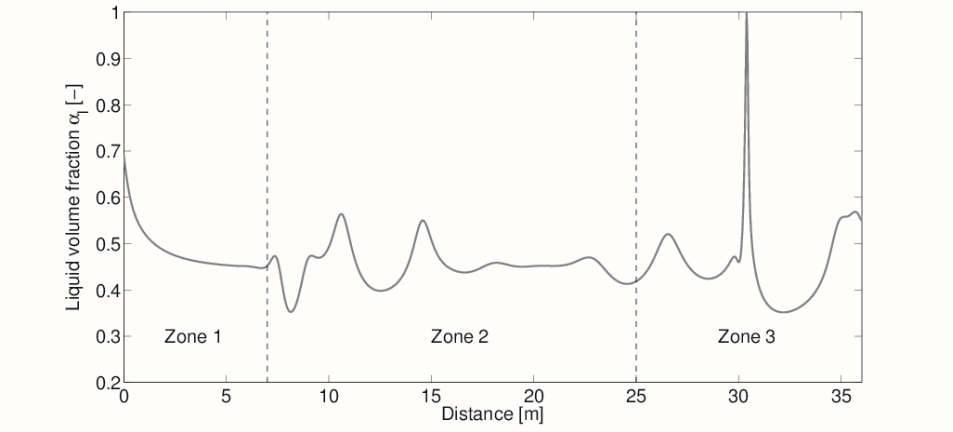

(b)

Figure 9. Slug initiation in *Pipe1* ($u_{gs} = 1.5\, m/s$ and $u_{ls} = 1.3\, m/s$) (**a**) and in *Pipe2* ($u_{gs} = 7.3\, m/s$ and $u_{ls} = 1.2\, m/s$) (**b**). The three zones of slug initiation proposed by \cite{Ansari1998} can be recognized in these numerical simulations.

5. VKH boundary: the neutral stability condition

We report here some details about how to compute the VKH boundary reported on the flow pattern maps. The neutral stability condition was not shown by [9] for this model: it is obtained from the dispersion equation for the case of zero-imaginary part of the complex propagation velocity ($\boldsymbol{C_i = 0}$, where $\boldsymbol{C = \omega/k}$, $\boldsymbol{\omega}$ is the complex angular velocity and k is the real wave number of the perturbation). In the limit of long wave hypothesis the effect of the numerical diffusivity vanishes and the neutral stability condition yield

$$C_{rn} = \frac{\omega}{k} = \frac{u_l\left(\frac{\partial D_2}{\partial u_l}\right)_{\alpha_l} - \alpha_l\left(\frac{\partial D_2}{\partial \alpha_l}\right)_{u_l}}{\left(\frac{\partial D_2}{\partial u_l}\right)_{\alpha_l}}, \tag{1}$$

$$C_{rn}^2 + C_{rn}(-u_l - A_{22}) + u_l A_{22} - \alpha_l A_{21}, \tag{2}$$

where $\boldsymbol{D_2}$, $\boldsymbol{A_{22}}$ and $\boldsymbol{A_{21}}$ are defined in Appendix B of the paper, $\boldsymbol{C_{rn}}$ is the neutral wave velocity given in an explicit expression. Eqs. (1) – (2) are used to compute the neutral stability boundary in term of superficial velocity map. The derivatives of Eq. (1) are computed numerically.

References

1. Coquel, F.; El Amine, K.; Godlewski, E.; Perthame, B.; Rascle, P. A numerical method using upwind schemes for the resolution of two-phase flows. *Journal of Computational Physics* **1997**, *136*, 272-288.
2. Paillére, H.; Corre, C.; Garcìa Cascales, J.R. On the extension of the AUSM+ scheme to compressible two-fluid models. *Computer and Fluids* **2003**, *32*, 891-916.
3. Zou, L.; Zhao, H.; Zhang, H. Solving phase appearance/disappearance two-phase flow problems with high resolution staggered grid and fully implicit schemes by the Jacobian-free Newton-Krylov Method. *Computer and Fluids* **2016**, *129*, 179-188.
4. Ferrari, M.; Bonzanini, A.; Poesio, P. A five-equation, transient, hyperbolic, one-dimensional model for slug capturing in pipes. *Int J Numer Meth Fluids* **2017** (in press).
5. Toro, E. F. *Riemann Solvers and Numerical Methods for Fluid Dinamycs*, 2nd ed.; Springer: Berlin, Germany, 1999; 3-540-65966-8.
6. Barnea, D.; Shoham, O.; Taitel, Y.; Dukler, A. E. Flow pattern transition for gas-liquid flow in horizontal and inclined pipes. Comparison of experimental data with theory. *Int Jou Multiphase Flow* ***1980***, *6*, 227-225.
7. Ansari, M. R. Dynamical behavior of slug initiation generated by short waves in two-phase air-water stratified flow. *ASME HTD* **1998**, *361*, 289-295.
8. Ansari, M. R.; Shokri, V. Numerical modeling of slug flow initiation in a horizontal channels using a two-fluid model. *Int Jou of Heat and Fluid Flow* **2011**, 32, 145-155.
9. Holmås, H.; Sira, T.; Nordsveen, M.; Langtangen, H. P.; Schulkes, R. Analysis of a 1D incompressible two-fluid model including artificial diffusion. *IMA Journal of Applied Mathematics* **2008**, *73*, 651-667.